







## Article

# Thermal behaviour of filatovite – a rare aluminarsenate mineral of the feldspar group

Liudmila A. Gorelova<sup>1</sup> , Oleg S. Vereshchagin<sup>1</sup> , Vladimir N. Bocharov<sup>1</sup>, Nadezhda V. Potekhina (née Shchipalkina)<sup>2</sup> ,  
Elena S. Zhitova<sup>3</sup>  and Igor V. Pekov<sup>2</sup>

<sup>1</sup>Saint Petersburg State University, University Emb. 7/9, 199034 St. Petersburg, Russia; <sup>2</sup>Faculty of Geology, Moscow State University, Vorobiev Gory, 119991 Moscow, Russia; and <sup>3</sup>Institute of Volcanology and Seismology FEB RAS, Boulevard Piip 9, 683006 Petropavlovsk-Kamchatsky, Russia

### Abstract

The high-temperature behaviour of a feldspar-group mineral, filatovite (with the simplified formula:  $K(\text{Al,Zn})_2(\text{As,Si})_2\text{O}_8$ ), in which the Al:As:Si ratio is close to 2:1:1), was studied by *in situ* high-temperature single-crystal X-ray diffraction and *in situ* high-temperature (hot stage) Raman spectroscopy up to 600°C. In the temperature range studied (25–600°C) filatovite does not undergo any phase transition, whereas at 800°C it decomposes to X-ray amorphous phase(s). The evolution of 12 main Raman bands was traced during heating, which indicates a gradual change in the crystal structure. The thermal expansion coefficients of filatovite demonstrate a sharply anisotropic character of thermal expansion: the maximal expansion is close to the *a* axis ( $\alpha_{11} = 17.7(1) \times 10^{-6} \text{ }^\circ\text{C}^{-1}$ ), whereas along the *b* and *c* axes the thermal expansion coefficients are close to zero. Such behaviour is typical for minerals with a similar crystal structure topology; it indicates the dominant role of structure geometry in the thermal behaviour of the mineral.

**Keywords:** filatovite; feldspar; thermal expansion; X-ray diffraction; Raman spectroscopy

(Received 10 August 2023; accepted 15 February 2024; Accepted Manuscript published online: 27 February 2024; Associate Editor: Oleg I Siidra)

### Introduction

Feldspar-group minerals (Krivovichev, 2020) are among the most widespread minerals in the Earth's crust, and they have been studied extensively under various pressure–temperature conditions (e.g. Smith and Brown, 1988; Parsons, 1994; Deer *et al.*, 2001; Bokii and Borutzkii, 2003; Henderson, 2021; Gorelova, 2023). The feldspar group includes 29 mineral species belonging to the aluminosilicate (the most widespread), borosilicate, beryllophosphate, ferrisilicate and aluminarsenate groups (Krivovichev, 2020). The aluminarsenate feldspar filatovite was first described by Vergasova *et al.* (2004), with the simplified formula  $K(\text{Al,Zn})_2(\text{As,Si})_2\text{O}_8$ , however this formula was later modified as follows:  $K(\text{Al}_{1+x}\text{M}_{1-x}^{2+})_{\Sigma 2}(\text{As}_{2-x}\text{Si}_x)_{\Sigma 2}\text{O}_8$  with  $\text{M}^{2+} = \text{Cu, Zn}$  and  $x < 1$  (Shchipalkina *et al.*, 2020a).

The crystal structure of filatovite was determined as monoclinic (Filatov *et al.*, 2004) based upon the three-dimensional framework of  $\text{TO}_4$  tetrahedra ( $T = \text{Si, Al}$  and  $\text{As}^{5+}$ ). This type of topology (feldspar topology; Krivovichev, 2020) is inherent to a series of widespread minerals (albite, anorthite, sanidine, orthoclase and microcline) as well as some rare minerals (rubicline, buddingtonite, celsian, reedmergnerite and ferrisanidine). Feldspar topology is one of the five possible topologies in the feldspar group of minerals, namely feldspar, paracelsian, svyatoslavite,

dmisteinbergite and hollandite (Krivovichev, 2020). The last two topologies differ from the other three significantly, as crystal structures with hollandite topologies are based upon  $\text{TO}_6$  octahedra, and crystal structures with dmisteinbergite topologies upon  $\text{TO}_4$  tetrahedra forming layers; whereas feldspar, paracelsian and svyatoslavite topologies are framework structures built of  $\text{TO}_4$  tetrahedra; they differ from each other only in the way the tetrahedra are connected.

It should be noted that filatovite has an almost unique chemical composition, containing Al, Si and As together as main constituents. Only eight minerals comprising meaningful amounts of these three elements are known to date (Table 1; more detailed description is provided in the Discussion). Due to the rarity of these minerals, they have not been studied under non ambient (extreme) conditions and the information about their thermal stability is limited to our knowledge of their formation conditions. Consequently, there are no data on the influence of the substitution of  $\text{Si}^{4+}$  for  $\text{As}^{5+}$  on the mineral stability. It is interesting that filatovite forms a continuous solid-solution series with sanidine (Shchipalkina *et al.*, 2020a). Moreover, this is the only example of a wide-ranging solid solution between (aluminosilicate and (aluminosilicate)arsenate minerals (Shchipalkina *et al.*, 2020a).

To date, filatovite has been found in only one locality, namely in fumaroles that have appeared as a result of the Great Fissure Tolbachik Eruption, Tolbachik volcano, Kamchatka peninsula, Russia (Vergasova *et al.*, 2004; Shchipalkina *et al.*, 2020b). According to Vergasova *et al.* (2004), the temperature of gases in filatovite-bearing fumaroles was  $\sim 410\text{--}420^\circ\text{C}$ , whereas Shchipalkina *et al.* (2020b) assumed that the temperature

**Corresponding author:** Liudmila A. Gorelova; Email: [lgorelova@spbu.ru](mailto:lgorelova@spbu.ru)

**Cite this article:** Gorelova L.A., Vereshchagin O.S., Bocharov V.N., Potekhina (née Shchipalkina) N.V., Zhitova E.S. and Pekov I.V. (2024) Thermal behaviour of filatovite – a rare aluminarsenate mineral of the feldspar group. *Mineralogical Magazine* 88, 176–184. <https://doi.org/10.1180/mgm.2024.10>

**Table 1.** List of IMA approved minerals, containing Al, Si, As and O together as the main constituents.

Name	Formula	Space group	Type locality	References*
Ardennite-(As)	$^{[5/7]}Mn_4^{[6]}Al_4^{[6]}(AlMg)^{[4]}(AsO_4)^{[4]}(SiO_4)_2^{[4]}(Si_3O_{10})(OH)_6$	<i>Pnmm</i>	Salmchâteau, Wallonia, Belgium	[1], [2]
Barrotite	$Cu_9Al(H^{[4]}SiO_4)_2[(^{[4]}SO_4)(H^{[4]}AsO_4)_{0.5}](OH)_{12} \cdot 8H_2O$	$P3_1$ or $P3_2$	Roua mine, Alpes-Maritimes, France	[3]
Carlfrancisite	$^{[4]}Mn_3^{[6]}(Mn,Mg,Al)_{42}^{[3]}(AsO_3)_2^{[4]}(AsO_4)_4^{[4]}(Si,As)O_{416}^{[4]}(As,Si)O_{412}^{[4]}(OH)_{42}$	<i>R3c</i>	Kombat mine, Otavi Valley, Namibia	[4]
Cervandonite-(Ce)	$^{[8]}(Ce,Nd,La)^{[6]}(Fe,Ti,Al)_3O_2^{[4]}(Si_2O_7)_{1-x+y}^{[3]}(AsO_3)_{1+x-y}(OH)_{3x-3y}$	<i>R3m</i>	Pizzo Cervandone, Binn Valley, Switzerland	[5], [6]
Filatovite	$^{[9]}Y^{[4]}(Al,Zn)_2^{[4]}(As,Si)_2O_8$	<i>I2/c</i>	Tolbachik volcano, Kamchatka, Russia	[7], [8]
Hundholmenite-(Y)	$^{[8/9/10]}(Y,Ln,Ca,Na)_{15}^{[6]}(Al,Fe)^{[10]}Ca_x^{[3]}As_{1-x}^{[4]}(Si,As)^{[4]}Si_6^{[4]}B_3(O,F)_{48}$	<i>R3m</i>	Hundholmen, Nordland County, Norway	[9]
Kraisslite	$^{[4]}Zn_3^{[6]}(Mn,Mg)_{25}^{[6]}(Fe,Al)^{[3]}(AsO_3)_2^{[4]}(Si,As)O_{410}(OH)_{16}$	$C222_1$	Sterling Hill mine, New Jersey, USA	[10], [11], [12]
Mcgovernite	$^{[4]}Zn_3^{[6]}(Mn,Mg,Fe,Al)_{42}^{[3]}(AsO_3)_2^{[4]}(AsO_4)_4^{[4]}(Si,As)O_{418}(OH)_{42}$	$R\bar{3}m$	Sterling Hill mine, New Jersey, USA	[11], [13]

\*References: [1] von Lasaulx (1872); [2] Barresi et al. (2007); [3] Sarp et al. (2014); [4] Hawthorne et al. (2013); [5] Armbruster et al. (1988); [6] Demartin et al. (2008); [7] Vergasova et al. (2004); [8] Filatov et al. (2004); [9] Raade et al. (2007); [10] Moore and Ito (1978); [11] Dunn and Nelen (1980); [12] Cooper and Hawthorne (2012); [13] Palache and Bauer (1927).

formation was not lower than 500°C. The temperature of filatovite formation could be even higher, as the temperature of the fumarole fields during the Tolbachik eruption was ~700°C (Menyalov et al., 1980).

The present study aims to investigate the high-temperature behaviour of filatovite using *in situ* high-temperature X-ray diffraction up to 800°C and *in situ* high-temperature (hot-stage) Raman spectroscopy up to 600°C in order to determine the stability temperatures of the mineral and the influence of As<sup>5+</sup> on the stability of feldspars.

**Materials and methods**

The sample of filatovite was collected from the Arsenatnaya fumarole, Second scoria cone of the North Breakthrough of the Great Fissure Tolbachik Eruption, Kamchatka peninsula, Russia. Six filatovite crystals were studied by scanning electron microscopy (SEM) with energy-dispersive X-ray spectroscopy (EDX). The crystal with the maximum arsenic content was epoxy-mounted, polished, carbon-coated and analysed using SEM with wavelength-dispersive X-ray spectroscopy (WDX). Next, the crystal (final size 30 × 10 × 10 µm) was extracted, polished by reactive ion etching with Ar<sup>+</sup> ions using an Oxford Instruments IonFab-300 instrument (500 V and 2.4 mA cm<sup>-2</sup> flow current),

studied using Raman spectroscopy, and then using single-crystal X-ray diffraction.

The chemical composition was determined using a S-3400N (Hitachi, Japan) SEM equipped with an Aztec Energy 350 (Oxford instruments, UK) EDX (SSD detector, accelerating voltage 20 kV, beam current 1 nA, and 1 µm beam diameter at the sample surface) and an Inca 500 (Oxford instruments, UK) WDX (accelerating voltage 20 kV, beam current 15 nA, and 3 µm beam diameter at the sample surface), using natural and synthetic standards. The empirical formula of filatovite (Table 2) was calculated on the basis of eight O atoms per formula unit (apfu).

High-temperature Raman spectroscopy studies in air were conducted up to 600°C with a temperature step of 50°C. The heating rate was ~25°C/min. Raman spectra of the sample were recorded from a single crystal in arbitrary orientation using a LabRam HR 800 spectrometer (Horiba Jobin-Yvon, Japan) equipped with a BX-41 (Olympus, Japan) microscope and a high-temperature attachment THMS600 System (Linkam, UK) in a back-scattering geometry system using a 532 nm laser. The Raman spectra were recorded in the range of 70–1800 cm<sup>-1</sup> at a

**Table 2.** Chemical composition of filatovite (No 1; our data) and As-rich potassic feldspar from the Arsenatnaya fumarole (No 2; Shchipalkina et al., 2020b).

Component	1	2
wt. %		
As <sub>2</sub> O <sub>5</sub>	37.04	36.00
P <sub>2</sub> O <sub>5</sub>	bdl	0.80
SiO <sub>2</sub>	18.78	19.19
Al <sub>2</sub> O <sub>3</sub>	31.50	30.70
Fe <sub>2</sub> O <sub>3</sub>	0.36	0.78
Na <sub>2</sub> O	0.27	0.41
K <sub>2</sub> O	13.51	12.67
Total	101.46	100.55
Formula calculated on the basis of 8 O apfu		
<i>T</i>		
As	1.03	1.00
P	–	0.04
Si	1.00	1.02
Al	1.97	1.92
Fe	0.01	0.03
<i>M</i>		
Na	0.03	0.04
K	0.91	0.86
Total <i>T</i> + <i>M</i>	4.95	4.91

Note: bdl – below detection limit

**Table 3.** Crystallographic data and refinement parameters for filatovite at different temperatures.

Temperature (°C)	27	200	400	600
<b>Crystal data</b>				
Space group	<i>I2/a</i>	<i>I2/a</i>	<i>I2/a</i>	<i>I2/a</i>
<i>a</i> (Å)	8.7661(3)	8.7896(3)	8.8174(4)	8.8448(4)
<i>b</i> (Å)	13.3428(4)	13.3411(5)	13.3375(6)	13.3335(5)
<i>c</i> (Å)	14.6781(6)	14.6916(7)	14.6784(9)	14.6837(8)
β (°)	115.893(3)	115.824(3)	115.831(4)	115.753(4)
Volume (Å <sup>3</sup> )	1544.5(1)	1550.7(1)	1553.7(2)	1559.7(1)
<i>Z</i>	8	8	8	8
<b>Data collection</b>				
Wavelength (Å)	0.71073	0.71073	0.71073	0.71073
Max. θ°	35.512	29.343	29.344	29.429
Index ranges	–14 ≤ <i>h</i> ≤ 14	–11 ≤ <i>h</i> ≤ 11	–11 ≤ <i>h</i> ≤ 11	–12 ≤ <i>h</i> ≤ 11
	–20 ≤ <i>k</i> ≤ 20	–17 ≤ <i>k</i> ≤ 18	–17 ≤ <i>k</i> ≤ 17	–18 ≤ <i>k</i> ≤ 17
	–23 ≤ <i>l</i> ≤ 22	–12 ≤ <i>l</i> ≤ 19	–19 ≤ <i>l</i> ≤ 15	–19 ≤ <i>l</i> ≤ 15
No. meas. refl.	19,001	6956	7264	7359
No. unique refl.	3288	1866	1841	1875
No. obs. refl. ( <i>I</i> > 2σ( <i>I</i> ))	2366	1340	1504	1453
<b>Refinement of the structure</b>				
No. of variables	124	124	118	118
<i>R</i> <sub>int</sub>	0.0663	0.0544	0.0416	0.0455
<i>R</i> <sub>1</sub> , all data	0.0849	0.0724	0.0797	0.0836
<i>R</i> <sub>1</sub> , <i>I</i> > 2σ( <i>I</i> )	0.0508	0.0422	0.0594	0.0584
w <i>R</i> <sub>2</sub> , all data	0.1083	0.1057	0.1311	0.1214
w <i>R</i> <sub>2</sub> , <i>I</i> > 2σ( <i>I</i> )	0.0980	0.0940	0.1233	0.1126
Goof	1.042	0.954	1.198	1.161

resolution of  $1\text{ cm}^{-1}$  and 20 s acquisition time and with the power at the sample of 10 mW. To improve the signal-to-noise ratio, the number of acquisitions was set to 50.

The thermal behaviour of filatovite under heating in air was also studied *in situ* by high-temperature single-crystal X-ray diffraction (SCXRD) using a XtaLAB Synergy-S diffractometer (Rigaku Oxford Diffraction, Japan) operated with monochromated  $\text{MoK}\alpha$  radiation ( $\lambda[\text{MoK}\alpha] = 0.71073\text{ \AA}$ ) at 50 kV and 1 mA and equipped with an HyPix-6000HE detector with a high-temperature FMB Oxford system (Oxford, UK). The sample was heated using a gas blower up to  $800 (\pm 10)\text{ }^\circ\text{C}$ . For the SCXRD study at all temperatures, the single crystal previously used for high-temperature Raman spectroscopy was used. First, this crystal was mounted on a polymer loop using paraton-*n* to collect diffraction data under ambient temperature. A hemisphere of diffraction data (with a frame width of  $0.5^\circ$ ) was collected. After that this crystal was mounted on a quartz fibre placed in a quartz capillary and fixed between the fibre and the capillary wall (see Gorelova *et al.*, 2021, for more details) to obtain SCXRD data under high-temperature conditions. High-temperature diffraction data were collected at 200, 400, 600 and  $800^\circ\text{C}$ . At each temperature the crystal was kept for  $\sim 10$  minutes prior to data collection.

It should be also noted, that at  $800^\circ\text{C}$ , the crystal turned out to be X-ray amorphous and the full SCXRD data were not collected at this temperature. For all other temperatures, a hemisphere of diffraction data (with a frame width of  $0.5^\circ$ ) was collected by analogy with the ambient temperature experiment. However, due to the instrumental feature of high-temperature experiments, namely a longer distance to the detector, when using the strategy similar to that used previously, the number of collected reflections is noticeably smaller. To avoid this discrepancy, the counting time was increased from 6 s for each frame at ambient temperature to 15 s under non-ambient conditions. Though the difference in the collected reflection was still large (see Table 3), no further increasing was possible. The data were integrated and corrected for background, Lorentz, and polarisation effects. The empirical absorption correction based on spherical harmonics implemented in the *SCALE3 ABSPACK* algorithm was applied in the *CrysAlisPro* program (Agilent Technologies, 2012). The unit-cell parameters were refined using the least-square techniques. The *SHELXL* program package (Sheldrick, 2008) was used for all structural calculations. All bond lengths in crystal structures at high temperatures were corrected for thermal vibrations of atoms according to the procedure described by Downs (2000)

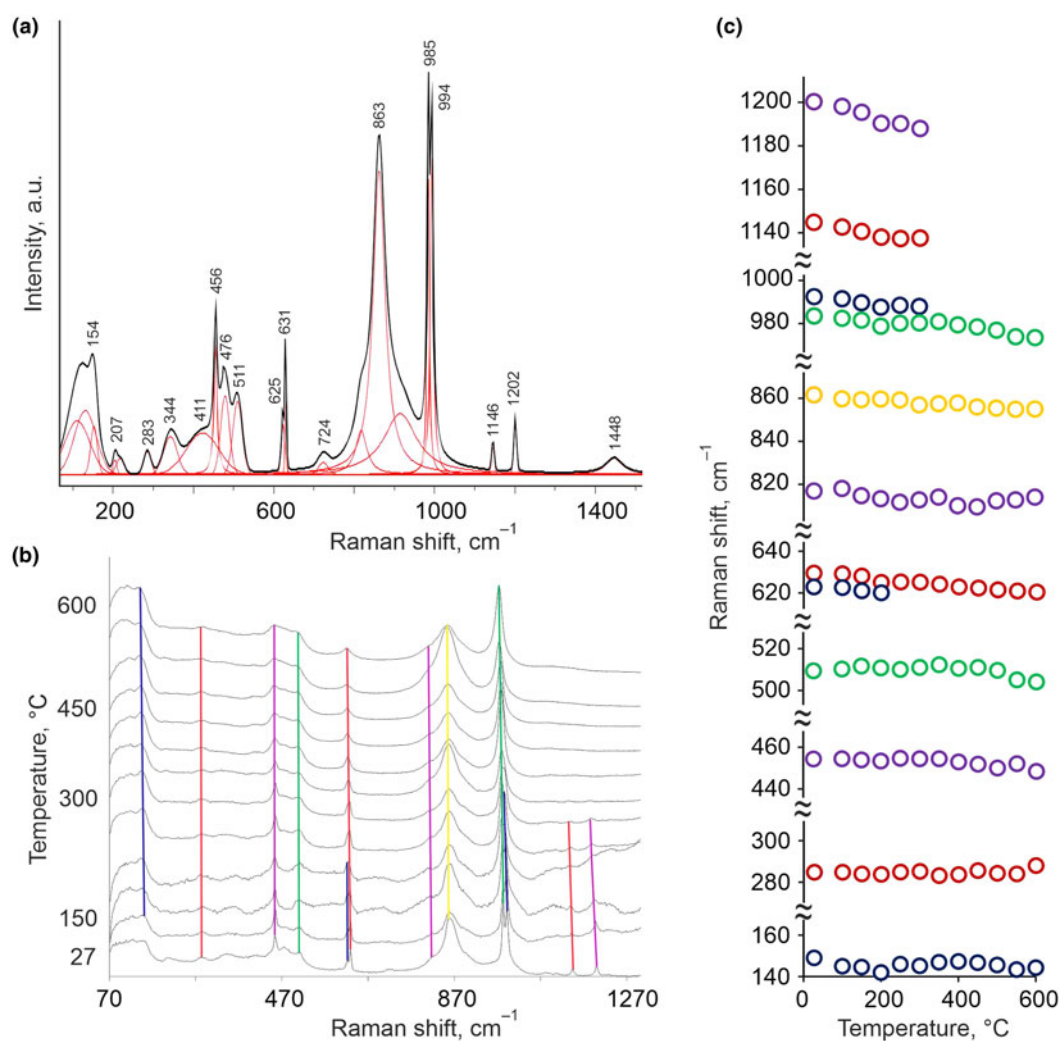


**Figure 1.** Raman spectra of filatovite (a) under ambient conditions; (b) at different temperatures from 70 to  $1500\text{ cm}^{-1}$ ; and (c) temperature evolution of 12 selected Raman bands. The errors are smaller than the size of the symbols.

and considering the  $8\pi^2$  difference between the  $U_{ij}$  and  $B_{ij}$  factors. The crystallographic information files have been deposited with the Principal Editor of *Mineralogical Magazine* and are available as Supplementary material (see below).

Due to the small number of experimental points, the temperature dependencies of the unit-cell parameters were described by linear polynomial functions up to 600°C, as the sample decomposed at 800°C (see below for more details). Using the approximation coefficient, the tensor component was determined in the Cartesian crystal-physical coordinate system as a solution of the system of six equations of the following form (Bubnova *et al.*, 2013):

$$\alpha_d = \alpha_{11}x_d^2 + \alpha_{22}y_d^2 + \alpha_{33}z_d^2 + 2\alpha_{12}x_dy_d + 2\alpha_{13}x_dz_d$$

where  $\alpha_{ij}$  are the tensor components and  $x_d$ ,  $y_d$  and  $z_d$  are the directional cosines of normal vectors with respect to the crystal-physical axes  $xyz$ . The thermal expansion along the normal vector to the  $(hkl)$  plane with the interplanar distance  $d_{hkl}$  was calculated as follows:

$$a_d = -\frac{d_{hkl}^2}{2} \cdot \left( \frac{\partial f}{\partial a} \cdot \frac{da}{dT} + \frac{\partial f}{\partial b} \cdot \frac{db}{dT} + \frac{\partial f}{\partial c} \cdot \frac{dc}{dT} + \frac{\partial f}{\partial \alpha} \cdot \frac{d\alpha}{dT} + \frac{\partial f}{\partial \beta} \cdot \frac{d\beta}{dT} + \frac{\partial f}{\partial \gamma} \cdot \frac{d\gamma}{dT} \right)$$

where  $d_{hkl}^2 = f(h, k, l, a, b, c, \alpha, \beta, \gamma)$  is a function of indices and unit-cell parameters. The standard orientation of the crystallographic axes with respect to the crystal-physical axes was used.

This procedure was performed using the *TTT* program package (Bubnova *et al.*, 2013), which was also used for the thermal-expansion parameter tensor visualisation.

## Results and discussion

### Chemical composition and Raman spectroscopy under ambient conditions

The chemical composition of filatovite is quite simple (Table 2), the Al:As:Si atomic ratio is close to 2:1:1. The crystal under study does not contain impurities of divalent cations (e.g. Cu and Zn), which is in a good agreement with the previous studies of As-rich feldspar from the Arsenatnaya fumarole (Shchipalkina *et al.*, 2020b). Potassium is the main extra-framework cation (0.91 apfu), while sodium is present in very small amounts (0.03 apfu).

The Raman spectrum of filatovite under ambient conditions (Fig. 1a) is in a good agreement with the published data on the sanidine–filatovite solid-solution series (Shchipalkina *et al.*, 2020a). The Raman band positions of the sample in question are very close to those of a sanidine–filatovite solid solution, whereas the intensity ratio is significantly different. Though the intensity of the Raman bands often depends strongly on the crystal orientation, the framework crystal structure of filatovite with different orientations of all structural units allows us to exclude the orientation influence.

In the sample studied, the three most intense bands with very close intensities are located in the region of 800–1000  $\text{cm}^{-1}$ , which is usually attributed to the symmetric stretching modes of  $TO_4$  tetrahedra. Based on literature data, the band at 863  $\text{cm}^{-1}$  is usually attributed to  $AsO_4$  tetrahedra (e.g. Botto and Baran, 1982; Vereshchagin *et al.*, 2019), whereas the bands at 985 and 994  $\text{cm}^{-1}$  are related to  $SiO_4$  and  $AlO_4$  tetrahedra (e.g. Dowty, 1987). The close intensities of the bands between 800 and 1000  $\text{cm}^{-1}$

**Table 4.** Bond distances in filatovite at different temperatures.

Bond distances (Å)	Temperature (°C)			
	27	200	400	600
<b><math>TO_4</math> tetrahedra (<math>T = \text{Si}</math> and <math>\text{As}</math>)</b>				
T1–O1	1.658(3)	1.656(3)	1.661(5)	1.661(5)
T1–O5	1.650(3)	1.652(4)	1.657(5)	1.659(4)
T1–O7	1.666(3)	1.670(3)	1.673(5)	1.680(5)
T1–O8	1.654(3)	1.653(5)	1.656(6)	1.656(6)
<T1–O>	1.657	1.658	1.662	1.664
T2–O2	1.655(3)	1.654(3)	1.651(4)	1.654(4)
T2–O3	1.648(3)	1.649(4)	1.647(5)	1.648(5)
T2–O4	1.660(2)	1.660(3)	1.667(5)	1.663(4)
T2–O6	1.653(4)	1.657(5)	1.661(7)	1.663(6)
<T2–O>	1.654	1.655	1.657	1.657
<b><math>AlO_4</math> tetrahedra</b>				
Al1–O1	1.760(3)	1.772(4)	1.767(5)	1.772(5)
Al1–O4	1.761(3)	1.761(3)	1.763(5)	1.767(5)
Al1–O7	1.749(3)	1.755(3)	1.755(5)	1.756(5)
Al1–O8	1.743(4)	1.755(6)	1.750(7)	1.756(7)
<Al1–O>	1.753	1.761	1.759	1.763
Al2–O2	1.764(3)	1.771(4)	1.774(4)	1.776(4)
Al2–O3	1.746(3)	1.751(3)	1.754(5)	1.759(5)
Al2–O5	1.757(3)	1.758(4)	1.762(6)	1.761(4)
Al2–O6	1.748(4)	1.756(5)	1.754(7)	1.756(6)
<Al2–O>	1.754	1.759	1.761	1.763
<b><math>MO_9</math> polyhedra (<math>M = \text{K}</math> and <math>\text{Na}</math>)</b>				
M–O1	3.205(3)	3.192(4)	3.186(5)	3.179(5)
M–O2	2.980(3)	2.997(5)	3.007(6)	3.017(6)
M–O3	3.162(3)	3.160(4)	3.153(5)	3.149(5)
M–O4	2.729(3)	2.747(4)	2.776(6)	2.797(5)
M–O5	2.917(3)	2.932(4)	2.958(5)	2.975(5)
M–O5a	2.983(3)	3.011(4)	3.034(5)	3.061(5)
M–O6	3.093(3)	3.101(5)	3.125(6)	3.139(6)
M–O7	2.999(4)	3.014(5)	3.017(6)	3.023(7)
M–O8	3.040(3)	3.055(5)	3.078(6)	3.097(6)
<M–O>	3.012	3.023	3.037	3.049

can indicate a high amount of As in the sample being considered (e.g.  $\sim\text{Si}:\text{As}$  ratio is 1:1), that is also confirmed by electron microprobe (see above) and SCXRD data (see below). In contrast, all the previously studied samples of the sanidine–filatovite solid-solution series with the maximum Si:Al ratio 1.61:0.63 have no intense band at  $\sim 863 \text{ cm}^{-1}$  (Shchipalkina *et al.*, 2020a). Weak bands in the region between 1000 and 1200  $\text{cm}^{-1}$  were also attributed to the asymmetric stretching modes of  $TO_4$  tetrahedra, according to the calculations (Shchipalkina *et al.*, 2020a). The band at 1448  $\text{cm}^{-1}$  can be presumably assigned to an overtone or combination mode.

The next group of medium intense bands is located between 400 and 700  $\text{cm}^{-1}$ , which were attributed to the ring breathing modes of four-membered rings of  $TO_4$  tetrahedra (Shchipalkina *et al.*, 2020a). It should be noted that the most intense band of the sample within this group of bands studied in this work is located at 456  $\text{cm}^{-1}$ , whereas in all the samples of sanidine–filatovite series studied previously, this band was less intense. The bands at 625 and 631  $\text{cm}^{-1}$  are mainly bending deformation of the tetrahedra, where the contribution of the aluminium to the vibration is predominant (Aliatis *et al.*, 2015).

Another group of bands with frequencies below 400  $\text{cm}^{-1}$ , responsible for the rotation–translation modes of four-membered rings and cage-shear modes, has no significant differences to the samples with a different Al:Si:As ratio (Shchipalkina *et al.*, 2020a).

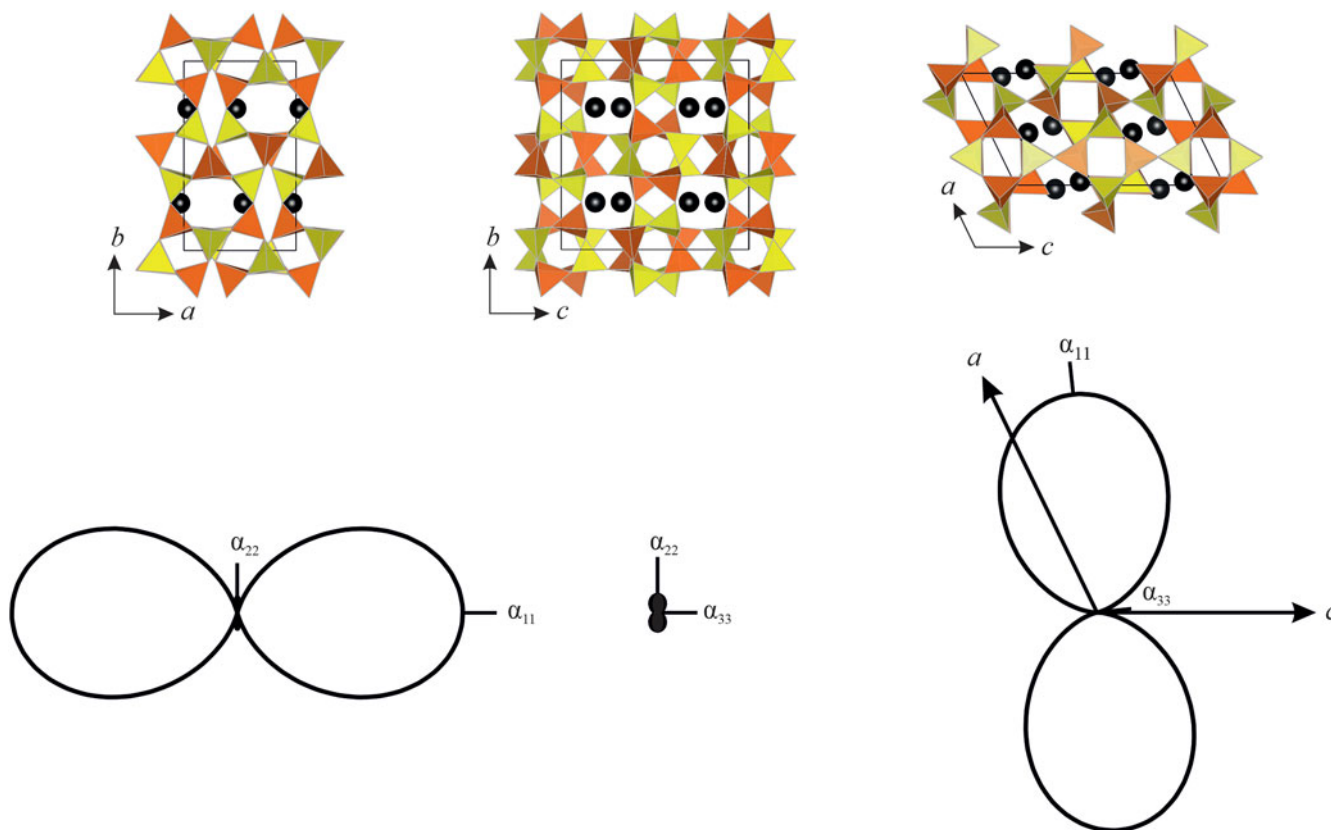


**Figure 2.** Crystal structure of filatovite in different projections with averaged thermal expansion section (black parts of the sections demonstrate the negative thermal expansion).  $\text{AlO}_4$  and  $(\text{Si,As})\text{O}_4$  tetrahedra are given in orange and yellow, respectively;  $M$  ( $M = \text{K}$  and  $\text{Na}$ ) atoms are shown as black displacement ellipsoids. The program package *Vesta* (Momma and Izumi, 2011) was used for crystal structure visualisation.

### Raman spectra evolution of filatovite upon heating

As the crystals of filatovite were small and the SCXRD study could not be performed at many temperatures, a high-temperature Raman spectroscopy study was undertaken for a quick evaluation of the high-temperature behaviour of filatovite, i.e. to determine the presence or absence of phase transformations. The evolution of 12 Raman bands upon heating was traced. Generally, all Raman bands moved to lower wavenumbers, i.e. underwent a red shift (Fig. 1c), which is typical for high-temperature conditions. Nevertheless, their shift speed was different: the bands in a low frequency number region (below  $500\text{ cm}^{-1}$ ) hardly changed their position across the whole temperature range, whereas the bands in a higher frequency number region, i.e. related to the deformations and vibrational stretching modes of  $\text{TO}_4$  tetrahedra, moved significantly. At first glance, it could be seen that there were abrupt changes at  $\sim 200$  and  $300^\circ\text{C}$ , but all these correspond to weak peaks and cannot be considered as structural changes. The disappearance of some peaks ( $\nu_5$ ,  $\nu_{10}$  and  $\nu_{11}$ ) refers to a general gradual deterioration of the Raman spectra upon heating (Fig. 1b).

### Crystal structure evolution and thermal expansion of filatovite upon heating

The crystal structure of filatovite was refined at four temperature points (Tables 3 and 4) including ambient conditions. According to SCXRD data, the  $M$  site is occupied by  $\text{K}$  and  $\text{Na}$  with a 9:1 ratio, two of four  $T$  sites are fully occupied by  $\text{Al}$ , whereas the

other two  $T$  sites are occupied by  $\text{Si}$  and  $\text{As}$  with a ratio close to 1:1 (e.g. the  $\text{Al}:\text{Si}:\text{As}$  ratio is 2:1:1). The bond lengths obtained are in a good agreement with the previous study of filatovite [our work vs Filatov *et al.*, 2004]:  $\langle T1-\text{O} \rangle = 1.657$  vs  $1.634\text{ \AA}$ ;  $\langle T2-\text{O} \rangle = 1.654$  vs  $1.634\text{ \AA}$ ;  $\langle \text{Al1}-\text{O} \rangle = 1.753$  vs  $1.753\text{ \AA}$ ;  $\langle \text{Al2}-\text{O} \rangle = 1.754$  vs  $1.754\text{ \AA}$ ; and  $\langle M-\text{O} \rangle = 3.012$  and  $3.020\text{ \AA}$ . Small differences in the tetrahedral bond length show there are slightly different  $\text{Al}:\text{As}:\text{Si}$  ratios in the crystals, which were studied by Filatov *et al.* (2004) (1.8:1.2:0.70) and in this work ( $\sim 2:1:1$ ), and that  $^{[4]}\text{Al} > ^{[4]}\text{As} > ^{[4]}\text{Si}$  (ionic radii are 0.39, 0.34 and  $0.26\text{ \AA}$ , respectively; Shannon, 1976). The shorter  $\text{Al}-\text{O}$  bonds in the crystal structure we studied are explained by the absence of  $\text{Zn}$  (ionic radii are 0.39 and  $0.6\text{ \AA}$  for  $\text{Al}$  and  $\text{Zn}$ , respectively; Shannon, 1976).

Attempts to refine the cation distribution by the sites at different temperatures lead to similar results at all temperatures, therefore they were fixed. This fact indicates the absence of the order-disorder process in the temperature range under consideration. Anisotropic displacement parameters were refined for all atoms at all temperatures.

As detailed above, filatovite belongs to minerals with feldspar topology (Krivovichev, 2020). Such crystal structures are described traditionally as consisting of so-called crankshaft chains of  $\text{TO}_4$  tetrahedra (in our case – alternate corner-sharing  $\text{AlO}_4$  and  $(\text{Si,As})\text{O}_4$  tetrahedra), formed by successive polymerisation of four-membered rings (Smith and Rinaldi, 1962; Smith, 1978). Such crankshaft chains in the crystal structure of filatovite are elongated along the  $a$  axis, and join together to form a three-dimensional framework (Fig. 2).

The temperature dependencies of the unit cell parameters are shown in Fig. 3. As there are only four experimental points, it is not possible to determine the existence of any phase transformation based on this graph only. Nevertheless, the crystal structure refinement at all temperatures clearly indicates the absence of phase transitions.

Due to the small number of experimental points, the thermal expansion coefficients were only calculated with a linear approximation of the temperature dependencies of the unit-cell parameters:  $\alpha_{11} = 17.7(1)$ ,  $\alpha_{22} = -1.2(1)$ ,  $\alpha_{33} = 0(1)$ ,  $\mu(\alpha_{11} \wedge a) = 19.7(5)$ ,  $\mu(\alpha_{33} \wedge c) = 6.2(5)$ ,  $\alpha_a = 15.70(4)$ ,  $\alpha_b = -1.2(1)$ ,  $\alpha_c = 0(1)$ ,  $\alpha_\beta = -1.8(5)$  and  $\alpha_V = 16(1) \times 10^{-6} \text{ }^\circ\text{C}^{-1}$ . In other words, the thermal expansion of filatovite has an extremely anisotropic character up to negative, and close to zero, expansion along the *b* and *c* axes (Fig. 2). The direction of the maximal thermal expansion is close to the *a* axis, i.e. along the crankshaft chain of  $\text{TO}_4$  tetrahedra. The  $\text{TO}_4$  ( $T = \text{Si}$  and  $\text{As}$ ) and  $\text{AlO}_4$  tetrahedra remain rigid upon heating; the bond lengths vary within 3 standard error(s) upon heating up to  $600^\circ\text{C}$  (Table 4). This is consistent with the data of Dove *et al.* (1993, 2000) and Palmer *et al.* (1997), which indicates the thermal stability of  $\text{TO}_4$  ( $T = \text{Si}$  and  $\text{Al}$ ) tetrahedra.

Though the crystal structure of filatovite does not undergo any polymorphic transformation, its deformation decreases. The two longest bonds ( $M\text{-O}1$  and  $M\text{-O}3$ ) in a  $\text{MO}_9$  polyhedron decrease upon heating, whereas all other bond lengths increase as temperature increases (Table 4, Fig. 4). The ( $M\text{-O}$ ) bond lengths change in the range of  $0.013\text{--}0.078 \text{ \AA}$  (Table 4). In other words, the  $\text{MO}_9$  polyhedron becomes more regular (less distorted) upon heating, which is also confirmed by the decrease of the polyhedron distortion index from 0.033 to 0.027 (calculated using the *Vesta* program package, Momma and Izumi, 2011).

It should also be noted that the direction of the maximal thermal expansion ( $\alpha_{11}$ ) is close to the direction of the minimal thermal vibration of the *M* cation regardless of temperature (Fig. 4b, c). A similar result was obtained previously for other alkaline feldspars (Filatov, 1990). This seemingly contradictory behaviour has been explained by the different nature of the factors determining thermal vibrations of atoms and thermal deformations of crystal structures (Filatov, 1990). Therefore, as it was mentioned above, the main factor determining the nature of thermal expansion of feldspar-related minerals is the crankshaft chain of  $\text{TO}_4$  tetrahedra and the framework topology, and not the extra-framework cation.

As mentioned above, the filatovite heating products were X-ray amorphous at  $800^\circ\text{C}$ , whereas at  $600^\circ\text{C}$  the mineral preserved crystallinity. Feldspar-bearing mineral assemblages in the Arsenatnaya and Yadovitaya fumaroles (including the one where filatovite was found) are thought to form at temperatures above  $500^\circ\text{C}$  (Pekov *et al.*, 2018). The synthetic analogue of filatovite was crystallised from the amorphous stoichiometric phase K ( $\text{Al}_2\text{AsSiO}_8$ ) at  $650^\circ\text{C}$  under atmospheric pressure (Kotelnikov *et al.*, 2019), which is consistent with our findings on the high temperature stability of filatovite. Thus, according to our investigation, we can conclude that the formation temperatures of this mineral is  $\sim 700 \pm 50^\circ\text{C}$ .

## Discussion

### Crystal chemistry of natural aluminoarsenicates

The chemical composition of filatovite is very specific, which is confirmed by the fact that, according to the Commission on

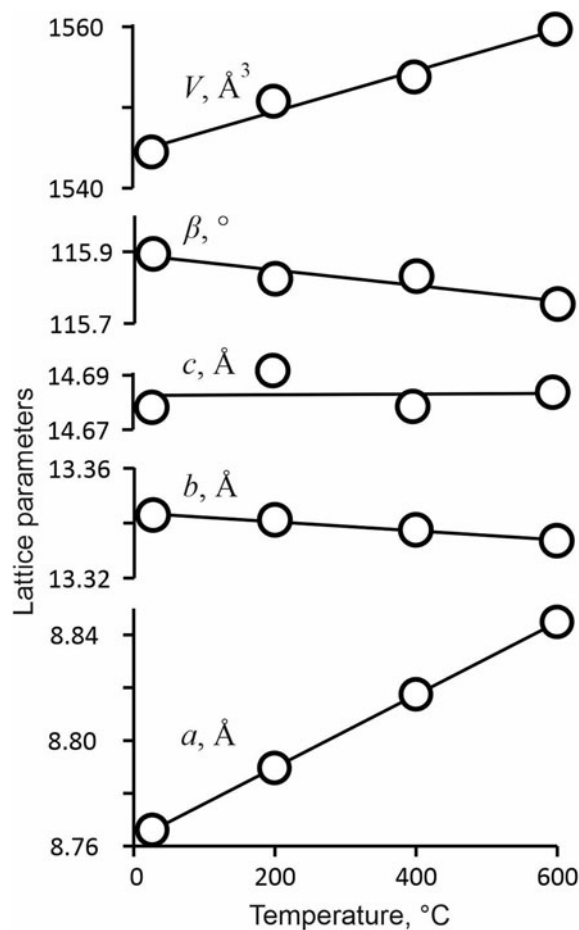
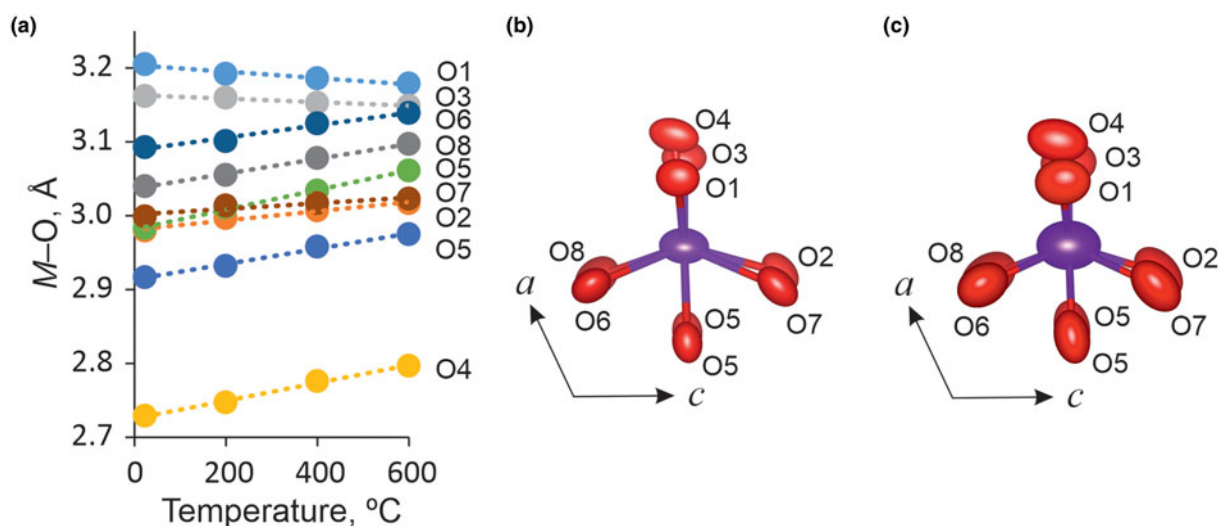


Figure 3. Unit-cell parameters of filatovite at different temperatures. Errors are smaller than symbols.

New Minerals, Nomenclature and Classification of the International Mineralogical Association (IMA–CNMNC, Pasero, 2024), only eight minerals containing significant amounts of Al, Si, As and O together are known to date (Table 1). All these minerals, except ardenite-(As), are extremely rare and are known from one to three localities each. Most of them are formed in very specific geological settings and originate in famous and geochemically unique deposits such as Långban in Sweden (Moore, 1970; Holtstam and Langhof, 1999; Christy and Gatedal, 2005) and Franklin and Sterling Hill in New Jersey, USA (Palache, 1941; Cook, 1973; Dunn, 1995).

From the crystal chemical point of view, all the minerals mentioned above differ significantly from filatovite, as only filatovite has Al, Si and As in tetrahedral coordination simultaneously. Ardenite-(As) and barrotite have Al in octahedral coordination (Donnay and Allmann, 1968 and Sarp *et al.*, 2014, respectively). Carlfrancisite, mcgovernite, hundholmenite-(Y), and kraisslite, have even more differences, because, in addition to  $\text{AlO}_6$  octahedra, they all also contain  $\text{As}^{3+}$  in triangular pyramidal coordination (Hawthorne, 2018; Raade *et al.*, 2007; Cooper and Hawthorne, 2012). Cervandonite-(Ce) has only silicon in tetrahedral coordination, whereas Al is in octahedra and  $\text{As}^{3+}$  in trigonal pyramidal coordination (Demartin *et al.*, 2008). In other words, filatovite is the only mineral, containing Al, Si and As in tetrahedral coordination.



**Figure 4.** Changes of the  $M-O$  bonds upon heating in (a)  $MO_3$  polyhedra and (b) the  $MO_3$  polyhedron in the ball-and-stick representation at 27°C and (c) 600°C. Red and purple ellipsoids show oxygen and  $M$  atoms, respectively.

### Thermal behaviour of feldspars isotypical to filatovite

As mentioned above, feldspar-group minerals, and especially those with feldspar topology, were studied in detail both under ambient and extreme (high-temperature and / or high-pressure) conditions (Parsons, 1994; Hovis *et al.*, 2008, 2010; Angel *et al.*, 2012; Pakhomova *et al.*, 2020; Henderson, 2021). According to Hovis *et al.* (2008, 2010), the thermal expansion behaviour of any feldspar (with feldspar topology) can be predicted if its chemical composition and unit cell volume under ambient conditions are known. Their conclusion was based on the idea, that all feldspars can be generally divided into two groups: (1)  $A^+AlSi_3O_8$  (' $AlSi_3$ '), where  $A$  are univalent alkali extra-framework cations and (2)  $B^{2+}Al_2Si_2O_8$  (' $Al_2Si_2$ '), where  $B$  are divalent alkali earth extra-framework cations. In terms of the framework architecture, filatovite is closer to the ' $Al_2Si_2$ ' type, whereas extra-framework cations are univalent alkali metals, so the prediction of its thermal expansion is a bit more difficult. Calculation of the volume thermal expansion coefficients for filatovite using the formulae for ' $AlSi_3$ ' and ' $Al_2Si_2$ ' feldspars, suggested by Hovis *et al.* (2008, 2010), gives a value of  $9.7$  and  $12.8 \times 10^{-6} \text{ }^\circ\text{C}^{-1}$ , respectively. As mentioned above, the experimental  $\alpha_V = 16(1) \times 10^{-6} \text{ }^\circ\text{C}^{-1}$ , i.e. the formula for ' $Al_2Si_2$ ' feldspar is more suitable for filatovite but it does not take into account all the crystal chemical features of filatovite. In order to find a more appropriate equation, it is necessary to study the thermal expansion of intermediate members of the sanidine–filatovite series.

We can conclude that the chemical composition of the framework has almost no influence on the volume thermal expansion orthoclase ( $\alpha_V = \sim 17 \times 10^{-6} \text{ }^\circ\text{C}^{-1}$ ; Henderson, 2021), microcline ( $\alpha_V = \sim 17 \times 10^{-6} \text{ }^\circ\text{C}^{-1}$ ; Openshaw *et al.*, 1979), sanidine ( $\alpha_V = \sim 21 \times 10^{-6} \text{ }^\circ\text{C}^{-1}$ ; Filatov, 1990) and filatovite ( $\alpha_V = 16(1) \times 10^{-6} \text{ }^\circ\text{C}^{-1}$ ), which have almost the same thermal expansion coefficients. This is in a good agreement with Hovis *et al.* (2010), who stated that the thermal expansion of framework feldspars with feldspar topology is determined primarily by the size of extra-framework cations.

The strong anisotropy of thermal expansion demonstrated by filatovite is typical for feldspar family minerals and synthetic compounds with alkali extra-framework cations (Henderson, 2021). The most probable reason for the sharp anisotropy of

filatovite thermal deformation is shear deformations caused by the intense increase of the  $M-O$  bond lengths, proposed by Filatov (1990) for feldspar-related minerals with feldspar topology. It should be noted that framework-type feldspar minerals with alkaline earth extra-framework cations demonstrated a much lower anisotropy degree (Henderson, 2021; Gorelova, 2023) compared to alkaline feldspars, regardless of framework topology.

**Acknowledgments.** The authors thank the X-ray Diffraction Centre, Centre for Geo-Environmental Research and Modelling (Geomodel) and Nanophotonics and Nanotechnology Resource Center of Saint Petersburg State University for providing instrumental and computational resources. This research was funded by the Russian Science Foundation, grant number 22-77-10033 (to L.A.G. and O.S.V.).

**Supplementary material.** The supplementary material for this article can be found at <https://doi.org/10.1180/mgm.2024.10>.

**Competing interests.** The authors declare none.

### References

- Agilent Technologies (2012) *CrysAlis PRO*. Agilent Technologies, Yarnton, Oxfordshire, UK.
- Aliatis I., Lambruschi E., Mantovani L., Bersani D., Ando S., Gatta G.D., Gentile P., Salvioli-Mariani E., Prencipe M., Tribaldino M. and Lottici P.P. (2015) A comparison between *ab initio* calculated and measured Raman spectrum of triclinic albite ( $NaAlSi_3O_8$ ). *Journal of Raman Spectroscopy*, **46**, 501–508.
- Angel R.J., Sochalski-Kolbus L.M. and Tribaldino M. (2012) Tilts and tetrahedra: the origin of the anisotropy of feldspars. *American Mineralogist*, **97**, 765–778.
- Armbruster T., Böhler C., Graeser S., Stalder H.A. and Amthauer G. (1988) Cervandonite-(Ce),  $(Ce,Nd,La)(Fe^{3+},Fe^{2+},Ti^{4+},Al)_3SiAs(Si,As)O_{13}$ , a new alpine fissure mineral. *Schweizerische Mineralogische und Petrographische Mitteilungen*, **68**, 125–132.
- Barresi A.A., Orlandi P. and Pasero M. (2007) History of ardenite and the new mineral ardenite-(V). *European Journal of Mineralogy*, **19**, 581–587.
- Bokii G.B. and Borutskii B.Ye. (editors) (2003) *Minerals. Vol. 5. Tectosilicates. Pt. 1: Silicates with interrupted framework, feldspar minerals*. Nauka, Moscow, 583 pp. [in Russian]

- Botto I.L. and Baran E.J. (1982) Characterization of the monoclinic rare earth orthoarsenates. *Journal of Less Common Metals*, **83**, 255–261.
- Bubnova R.S., Firsova V.A. and Filatov S.K. (2013) Software for determining the thermal expansion tensor and the graphic representation of its characteristic surface (Theta to Tensor-TTT). *Glass Physics and Chemistry*, **39**, 347–350.
- Christy A.G. and Gatedal K. (2005) Extremely Pb-rich rock-forming silicates including a beryllian scapolite and associated minerals in a skarn from Långban, Värmland, Sweden. *Mineralogical Magazine*, **69**, 995–1018.
- Cook D.K. (1973) Recent work on the minerals of Franklin and Sterling Hill, New Jersey. *Mineralogical Record*, **4**, 62–66.
- Cooper M.A. and Hawthorne F.C. (2012) Crystal structure of kraisslite,  $Zn_3(Mn,Mg)_2(Fe^{3+},Al)(As^{3+}O_3)_2[(Si,As^{5+})O_4]_{10}(OH)_{16}$ , from the Sterling Hill mine, Ogdensburg, Sussex County, New Jersey, USA. *Mineralogical Magazine*, **76**, 2819–2836.
- Deer W.A., Howie R.A. and Zussman J. (2001) *Rock-Forming Minerals. Vol. 4A. Framework Silicates: Feldspars*. The Geological Society, London, 973 pp.
- Demartin F., Gramaccioli C.M. and Graeser S. (2008) The crystal structure of cervandonite-(Ce), an interesting example of  $As^{3+}$ -Si diadochy. *The Canadian Mineralogist*, **46**, 423–430.
- Donnay G. and Allmann R. (1968)  $Si_3O_{10}$  groups in the crystal structure of ardenite. *Acta Crystallographica*, **B24**, 845–855.
- Dove M.T., Cool T., Palmer D.C., Putnis A., Salje H. and Winkler B. (1993) On the role of Al–Si ordering in the cubic-tetragonal phase transition of leucite. *American Mineralogist*, **78**, 486–492.
- Dove M.T., Pride A.K.A. and Keen D.A. (2000) Phase transitions in tridimite studied using ‘Rigid Unit Mode’ theory, reverse Monte Carlo methods and molecular dynamics simulations. *Mineralogical Magazine*, **64**, 267–283.
- Downs R.T. (2000) Analysis of harmonic displacement factors. Pp. 61–187 in: *High-Temperature and High Pressure Crystal Chemistry* (R.M. Hazen and R.T. Downs, editors). Reviews in Mineralogy and Geochemistry, Vol. 41. Mineralogical Society of America, Geochemical Society, Washington DC.
- Dowty E. (1987) Vibrational interactions of tetrahedra in silicate glasses and crystals - I. calculations on ideal silicate-aluminate-germanate structural units. *Physics and Chemistry of Minerals*, **14**, 542–552.
- Dunn P.J. (1995) *Franklin and Sterling Hill, New Jersey: The World’s Most Magnificent Mineral Deposits*. Franklin-Ogdensburg Mineralogical Society, New Jersey, USA, 755 pp.
- Dunn P.J. and Nelen J.A. (1980) Kraisslite and mcgovernite: new chemical data. *American Mineralogist*, **65**, 957–960.
- Filatov S.K. (1990) *High-Temperature Crystal Chemistry*. Nedra, Leningrad, Russia, 288 pp. [in Russian].
- Filatov S.K., Krivovichev S.V., Burns P.C. and Vergasova L.P. (2004) Crystal structure of filatovite,  $K((Al,Zn)_2(As,Si)_2O_8)$ , the first arsenate of the feldspar group. *European Journal of Mineralogy*, **16**, 537–543.
- Gorelova L.A. (2023) Phase transformations in feldspar group minerals with paracelsian topology under high temperature and high pressure. *Russian Geology and Geophysics*, **64**, 1–12.
- Gorelova L., Vereshchagin O. and Kasatkin A. (2021) Thermal expansion and polymorphism of slawsonite  $SrAl_2Si_2O_8$ . *Minerals*, **11**, 1150.
- Hawthorne F.C. (2018) Long-range and short-range cation order in the crystal structures of carlfrancisite and mcgovernite. *Mineralogical Magazine*, **82**, 1101–1118.
- Hawthorne F.C., Abdu Y.A., Ball N.A. and Pinch W.W. (2013) Carlfrancisite:  $Mn_3^{2+}(Mn^{2+},Mg,Fe^{3+},Al)_{42}(As^{3+}O_3)_2(As^{5+}O_4)_4[(Si,As^{5+})O_4]_6[(As^{5+},Si)O_4]_2(OH)_{42}$ , a new arseno-silicate mineral from the Kombat mine, Otavi Valley, Namibia. *American Mineralogist*, **98**, 1693–1696.
- Henderson C.M.B. (2021) Composition, thermal expansion and phase transitions in framework silicates: Revisitation and review of natural and synthetic analogues of nepheline-, feldspar- and leucite-mineral groups. *Solids*, **2**, 1–49.
- Holtstam D. and Langhof J. (1999) *Långban: The Mines, Their Minerals, Geology and Explorers*. Raset Förlag, Chr. Weise Verlag, Munich and Swedish Museum of Natural History, Stockholm, 216 pp.
- Hovis G.L., Medford A., Conlon M., Tether A. and Romanoski A. (2010) Principles of thermal expansion in the feldspar system. *American Mineralogist*, **95**, 1060–1068.
- Hovis G.L., Morabito J.R., Spooner A., Mott A., Person E.L., Henderson C.M.B., Roux J. and Harlov D. (2008) A simple predictive model for the thermal expansion of  $AlSi_3$  feldspars. *American Mineralogist*, **93**, 1568–1573.
- Kotelnikov A.R., Shchipalkina N.V., Suk N.I. and Ananiev V.V. (2019) Synthesis of As-bearing feldspar. *Proceedings of the X International Symposium “Mineral diversity: research and preservation”*. Sofia, October 2019.
- Krivovichev S.V. (2020) Feldspar polymorphs: Diversity, complexity, stability. *Zapiski RMO Proceedings of Russian Mineralogical Society*, **149**, 16–66.
- Menyalov I.A., Nikitina L.P. and Shapar’ V.N. (1980) *Geochemical Features of Exhalations of the Great Tolbachik Fissure Eruption*. Nauka, Moscow, 236 pp. [in Russian].
- Momma K. and Izumi F. (2011) VESTA 3 for three-dimensional visualization of crystal, volumetric and morphology data. *Journal of Applied Crystallography*, **44**, 1272–1276.
- Moore P.B. (1970) Mineralogy and chemistry of Langban-type deposits in Bergslagen, Sweden. *Mineralogical Record*, **1**, 154–172.
- Moore P.B. and Ito J. (1978) Kraisslite, a new platy arsenosilicate from Sterling Hill, New Jersey. *American Mineralogist*, **63**, 938–940.
- Openshaw R.E., Henderson C.M.B. and Brown W.L. (1979) A room-temperature phase transition in maximum microcline. *Physics and Chemistry of Minerals*, **5**, 95–104.
- Pakhomova A., Simonova D., Koemets I., Koemets E., Aprilis G., Bykov M., Gorelova L., Fedotenko T., Prakupenka V. and Dubrovinsky L. (2020) Polymorphism of feldspars above 10 GPa. *Nature Communications*, **11**, 2721.
- Palache C. (1941) Contributions to the mineralogy of Sterling Hill, New Jersey: Morphology of graphite, arsenopyrite, pyrite and arsenic. *American Mineralogist*, **26**, 709–717.
- Palache C. and Bauer L.H. (1927) McGovernite, a new mineral from Sterling Hill, New Jersey. *American Mineralogist*, **12**, 373–374.
- Palmer D.C., Dove M.T., Ibberson R.M. and Powell B.M. (1997) Structural behavior, crystal chemistry, and phase transitions in substituted leucite: High resolution neutron powder diffraction studies. *American Mineralogist*, **82**, 16–29.
- Parsons I. (1994) *Feldspars and Their Reactions*. Kluwer Academic Publishers: Amsterdam, The Netherlands, 650 pp.
- Pasero M. (2024) *The New IMA List of Minerals. International Mineralogical Association. Commission on new minerals, nomenclature and classification (IMA-CNMNC)*. <http://cnmnc.units.it/> [Accessed February, 2024].
- Pekov I.V., Koshlyakova N.N., Zubkova N.V., Lykova I.S., Britvin S.N., Yapaskurt V.O., Agakhanov A.A., Shchipalkina N.V., Turchkova A.G. and Sidorov E.G. (2018) Fumarolic arsenates — a special type of arsenic mineralization. *European Journal of Mineralogy*, **30**, 305–322.
- Raade G., Johnsen O., Erambert M. and Petersen O.V. (2007) Hundholmenite-(Y) from Norway — a new mineral species in the vicinite group: descriptive data and crystal structure. *Mineralogical Magazine*, **71**, 179–192.
- Sarp H., Černý R., Pushcharovsky D.Y., Schouwink P., Teyssier J., Williams P.A., Babalik H. and Mari G. (2014) La barrotite,  $Cu_9Al(HSiO_4)_2[(SO_4)(HAsO_4)_{0.5}](OH)_{12} \cdot 8H_2O$ , un nouveau minéral de la mine de Roua (Alpes-Maritimes, France). *Riviera Scientifique*, **98**, 3–22.
- Shannon R.D. (1976) Revised effective ionic radii and systematic study of inter atomic distances in halides and chalcogenides. *Acta Crystallographica*, **A32**, 751–767.
- Shchipalkina N.V., Pekov I.V., Britvin S.N., Koshlyakova N.N. and Sidorov E.G. (2020a) Arsenic and phosphorus in feldspar framework: sanidine – filatovite solid solution series from fumarolic exhalations of the Tolbachik volcano, Kamchatka, Russia. *Physics and Chemistry of Minerals*, **47**, 1.
- Shchipalkina N.V., Pekov I.V., Koshlyakova N.N., Britvin S.N., Zubkova N.V., Varlamov D.A. and Sidorov E.G. (2020b) Unusual silicate mineralization in fumarolic sublimates of the Tolbachik volcano, Kamchatka, Russia – Part 2: Tectosilicates. *European Journal of Mineralogy*, **32**, 121–136.
- Sheldrick G.M. (2008) A short history of SHELX. *Acta Crystallographica*, **A64**, 112.
- Smith J.V. (1978) Enumeration of 4-connected 3-dimensional nets and classification of framework silicates. II. Perpendicular and near-perpendicular linkages from  $4.8^2$ ,  $3.12^2$  and  $4.6.12$  nets. *American Mineralogist*, **63**, 960–969.



- Smith J.V. and Brown W.L. (1988) *Feldspar Minerals. Vol. 1. Crystal Structures, Physical, Chemical and Microstructural Properties*. Springer Verlag, Berlin-Heidelberg, 828 pp.
- Smith J.V. and Rinaldi F. (1962) Framework structures formed from parallel four- and eight-membered rings. *Mineralogical Magazine*, **33**, 202–212.
- Vereshchagin O.S., Britvin S.N., Perova E.N., Brusnitsyn A.I., Polekhovskiy Y.S., Shilovskikh V.V., Bocharov V.N., van der Burgt A., Cuchet S. and Meisser N. (2019) Gasparite-(La),  $\text{La}(\text{AsO}_4)$ , a new mineral from Mn ores of the Ushkatyn-III deposit, Central Kazakhstan, and metamorphic rocks of the Wann Glacier, Switzerland. *American Mineralogist*, **104**, 1469–1480.
- Vergasova L.P., Krivovichev S.V., Britvin S.N., Burns P.C. and Ananiev V.V. (2004) Filatovite,  $\text{K}[(\text{Al}, \text{Zn})_2(\text{As}, \text{Si})_2\text{O}_8]$ , a new mineral species from the Tolbachik volcano, Kamchatka peninsula, Russia. *European Journal of Mineralogy*, **16**, 533–536.
- von Lasaulx A. (1872) Ardenit, ein neues Mineral. *Neues Jahrbuch für Mineralogie, Geologie und Paläontologie*, **1872**, 930–934.